JCI insight

High-dimensional analysis reveals a pathogenic role of inflammatory monocytes in experimental diffuse alveolar hemorrhage

Pui Y. Lee, … , Westley H. Reeves, Peter A. Nigrovic

JCI Insight. 2019;4(15):e129703. https://doi.org/10.1172/jci.insight.129703.

Research Article **Pulmonology**

Diffuse alveolar hemorrhage (DAH) is a life-threatening pulmonary complication associated with systemic lupus erythematosus, vasculitis, and stem cell transplant. Little is known about the pathophysiology of DAH, and no targeted therapy is currently available. Pristane treatment in mice induces systemic autoimmunity and lung hemorrhage that recapitulates hallmark pathologic features of human DAH. Using this experimental model, we performed high-dimensional analysis of lung immune cells in DAH by mass cytometry and single-cell RNA sequencing. We found a large influx of myeloid cells to the lungs in DAH and defined the gene expression profile of infiltrating monocytes. Bone marrow–derived inflammatory monocytes actively migrated to the lungs and homed adjacent to blood vessels. Using 3 models of monocyte deficiency and complementary transfer studies, we established a central role of inflammatory monocytes in the development of DAH. We further found that the myeloid transcription factor interferon regulatory factor 8 is essential to the development of both DAH and type I interferon–dependent autoimmunity. These findings collectively reveal monocytes as a potential treatment target in DAH.

JCI insight

RESEARCH ARTICLE

High-dimensional analysis reveals a pathogenic role of inflammatory monocytes in experimental diffuse alveolar hemorrhage

Pui Y. Lee,[1,2] Nathan Nelson-Maney,[2] Yuelong Huang,[2] Anaïs Levescot,[2] Qiang Wang,[2] Kevin Wei,[2] Pierre Cunin,[2] Yi Li,[3] James A. Lederer,[4] Haoyang Zhuang,[5] Shuhong Han,[5] Edy Y. Kim,[6] Westley H. Reeves,[5] and Peter A. Nigrovic[1,2]

[1]Division of Immunology, Boston Children's Hospital, Boston, Massachusetts, USA. [2]Division of Rheumatology, Immunology and Allergy, Brigham and Women's Hospital, Boston, Massachusetts, USA. [3]Division of Rheumatology, Beth Israel Deaconess Hospital, Boston, Massachusetts, USA. [4]Center for Data Sciences, Brigham and Women's Hospital and Harvard Medical School, Boston, Massachusetts, USA. [5]Division of Rheumatology, University of Florida College of Medicine, Gainesville, Florida, USA. [6]Department of Pulmonary and Critical Care Medicine, Brigham and Women's Hospital, Boston, Massachusetts, USA.

Diffuse alveolar hemorrhage (DAH) is a life-threatening pulmonary complication associated with systemic lupus erythematosus, vasculitis, and stem cell transplant. Little is known about the pathophysiology of DAH, and no targeted therapy is currently available. Pristane treatment in mice induces systemic autoimmunity and lung hemorrhage that recapitulates hallmark pathologic features of human DAH. Using this experimental model, we performed high-dimensional analysis of lung immune cells in DAH by mass cytometry and single-cell RNA sequencing. We found a large influx of myeloid cells to the lungs in DAH and defined the gene expression profile of infiltrating monocytes. Bone marrow–derived inflammatory monocytes actively migrated to the lungs and homed adjacent to blood vessels. Using 3 models of monocyte deficiency and complementary transfer studies, we established a central role of inflammatory monocytes in the development of DAH. We further found that the myeloid transcription factor interferon regulatory factor 8 is essential to the development of both DAH and type I interferon–dependent autoimmunity. These findings collectively reveal monocytes as a potential treatment target in DAH.

Introduction

Diffuse alveolar hemorrhage (DAH) is a life-threatening pulmonary complication of systemic lupus erythematosus (SLE) and other autoimmune diseases (1). DAH occurs in about 4% of patients with lupus and may represent the presenting manifestation of SLE (2). In the absence of targeted therapy, aggressive immunosuppression with corticosteroids, cyclophosphamide, rituximab, or plasma exchange remains the mainstay of treatment in DAH (3). Despite these measures, many patients experience relapse, and the overall mortality rate of DAH in SLE is greater than 30% (2, 4, 5). The inciting pathology is not clear, but involvement of microvascular inflammation (pulmonary capillaritis) and variable association with autoantibodies and complement deposition have been described (6–8). The interplay of immune cells that elicits local inflammation and tissue destruction in the lungs has not been examined in detail.

Although many animal models have been established to study the pathogenesis of SLE, only the pristane-induced model of autoimmunity manifests pulmonary hemorrhage (9). Mice treated intraperitoneally (i.p.) with the hydrocarbon pristane (also known as tetramethylpentadecane) develop chronic peritoneal inflammation and many features of human SLE, including autoantibodies against nucleic acids and ribonuclear proteins, glomerulonephritis, and the type I interferon signature (10–12). Interestingly, a single dose of pristane also induces DAH within 2 weeks (13, 14). More than 75% of wild-type (WT) C57BL/6 mice develop DAH, and about 20% succumb to fulminant hemorrhage. Histologically, pristane-induced DAH recapitulates hallmark features of human DAH, including pulmonary capillaritis (14, 15).

Authorship note: PYL and NNM contributed equally to this work.

Conflict of interest: The authors have declared that no conflict of interest exists.

Submitted: April 19, 2019
Accepted: June 27, 2019
Published: August 8, 2019.

Reference information: *JCI Insight*. 2019;4(15):e129703. https://doi.org/10.1172/jci.insight.129703.

How pristane drives the development of DAH remains unclear. Although pristane-induced lupus is dependent on interferon type I (IFN-I) production downstream of Toll-like receptor 7 (Tlr7), mice with defective Tlr7 or IFN-I signaling remain susceptible to DAH (15, 16). TNF-α signaling does not contribute to DAH development while IL-10 may have a protective role. IgM and complement C3 are required for the development of lung hemorrhage, suggesting a role of complement-mediated vasculitis (13, 15).

The pulmonary cell infiltrate in pristane-treated mice has not been well characterized. Although lymphoid and myeloid cell subsets can be delineated by fluorescence-based flow cytometry in healthy lung tissue, unambiguous identification of immune cells in hemorrhagic lung tissue is challenged by limitations in spectral overlap and presence of autofluorescence from large phagocytic cells and cellular debris. Mass cytometry is a recently described flow cytometry technique based on conjugation of heavy metal isotopes to antibodies and quantification by time-of-flight mass spectrometry (17). This technique allows simultaneous analysis of a large number of cellular markers without the limitations imposed by cell size, autofluorescence, or spectral overlap (17, 18).

In this study, we combined mass cytometry with single-cell RNA sequencing (scRNA-Seq) to study the pulmonary immune cell infiltrate of pristane-treated mice. Using high-dimensional analysis of myeloid cells with confirmatory in vivo studies using transgenic mouse strains and cell transfer, we define a critical role of monocytes in the pathogenesis of DAH.

Results

High-dimension analysis of immune cells in DAH by mass cytometry. DAH can be modeled experimentally in C57BL/6 mice by a single injection of pristane (14). Within 2 weeks of pristane treatment, lung hemorrhage occurred in more than 70% of mice, with severity ranging from mild focal hemorrhage to fulminant DAH (Figure 1A). Microscopically, DAH was characterized by extravasation of erythrocytes and leukocytes to the alveolar space and bronchioles, with widespread deposition of hemosiderin (Figure 1B). Given the acute onset of pathology, we hypothesized that the inflammatory process leading to DAH likely involves the innate immune system. However, the development of DAH was not dependent on TLR signaling components (Tlr7, Tlr9, Myd88, and Trif), IL-1α/β, ST2 (receptor for IL-33), TNF-α, or Fc receptor γ chain (Supplemental Figure 1A; supplemental material available online with this article; https://doi.org/10.1172/jci.insight.129703DS1).

Immune cells that infiltrate the lungs during DAH have not been well characterized in patients or in mice. Precise analysis by flow cytometry is hindered by the autofluorescence associated with pristane-induced DAH, especially when multiple channels were required to determine cell identity (Supplemental Figure 1B). To circumvent this issue, we performed mass cytometry on digested lung tissue based on methods described by Becher and colleagues (18) using the gating strategies illustrated in Supplemental Figure 1C.

viSNE (t-distributed stochastic neighbor embedding–based visualization) analysis of viable $CD45^+$ cells from digested lung tissue of PBS- and pristane-treated mice revealed significant differences in the distribution of immune cells (Figure 1, C and D). Cell populations on the viSNE plot were identified by differential expression of individual lineage markers (Figure 1E). Pristane treatment was associated with a large expansion of neutrophils and other $CD11b^+$ myeloid cells while B lymphocytes and Siglec-F^+CD11c^+ alveolar macrophages were reduced. After adjusting for the approximate 2.5-fold increase in total lung leukocytes in mice with DAH, the difference in myeloid cells was more prominent while lymphocyte number was less affected (Supplemental Figure 2, A and B). The inverse correlation between infiltrating myeloid cells and Siglec-F^+ cells in DAH was also confirmed by confocal microscopy (Figure 1F). Curiously, the accumulation of $CD11b^+$ myeloid cells and depletion of alveolar macrophages ($CD11c^+$Siglec-F^+) both correlated with the severity of DAH (Figure 1G). In contrast, changes in lymphocyte populations were not associated with severity of DAH (Supplemental Figure 2C).

Enrichment of bone marrow–derived myeloid cells in DAH. The lungs possess a variety of myeloid lineages, including granulocytes, monocytes, macrophages, and dendritic cells (DCs). To better define the myeloid populations that infiltrate the lungs in DAH, we performed focused viSNE analysis by excluding lymphocytes (Figure 2A). We unambiguously identified a marked increase of neutrophils, $Ly6C^{hi}$ "inflammatory" monocytes, and $Ly6C^{lo}$ "patrolling" monocytes in pristane-treated mice, while interstitial macrophages increased slightly (Figure 2, A–C, and Supplemental Figure 2, D and E). DC subsets were minimally affected compared to PBS-treated controls. We also performed spanning-tree progression analysis of density-normalized events (SPADE) analysis of the mass cytometry data (19). Using CD11b as a marker to discriminate infiltrating myeloid cells, SPADE display similarly demonstrated an expansion of

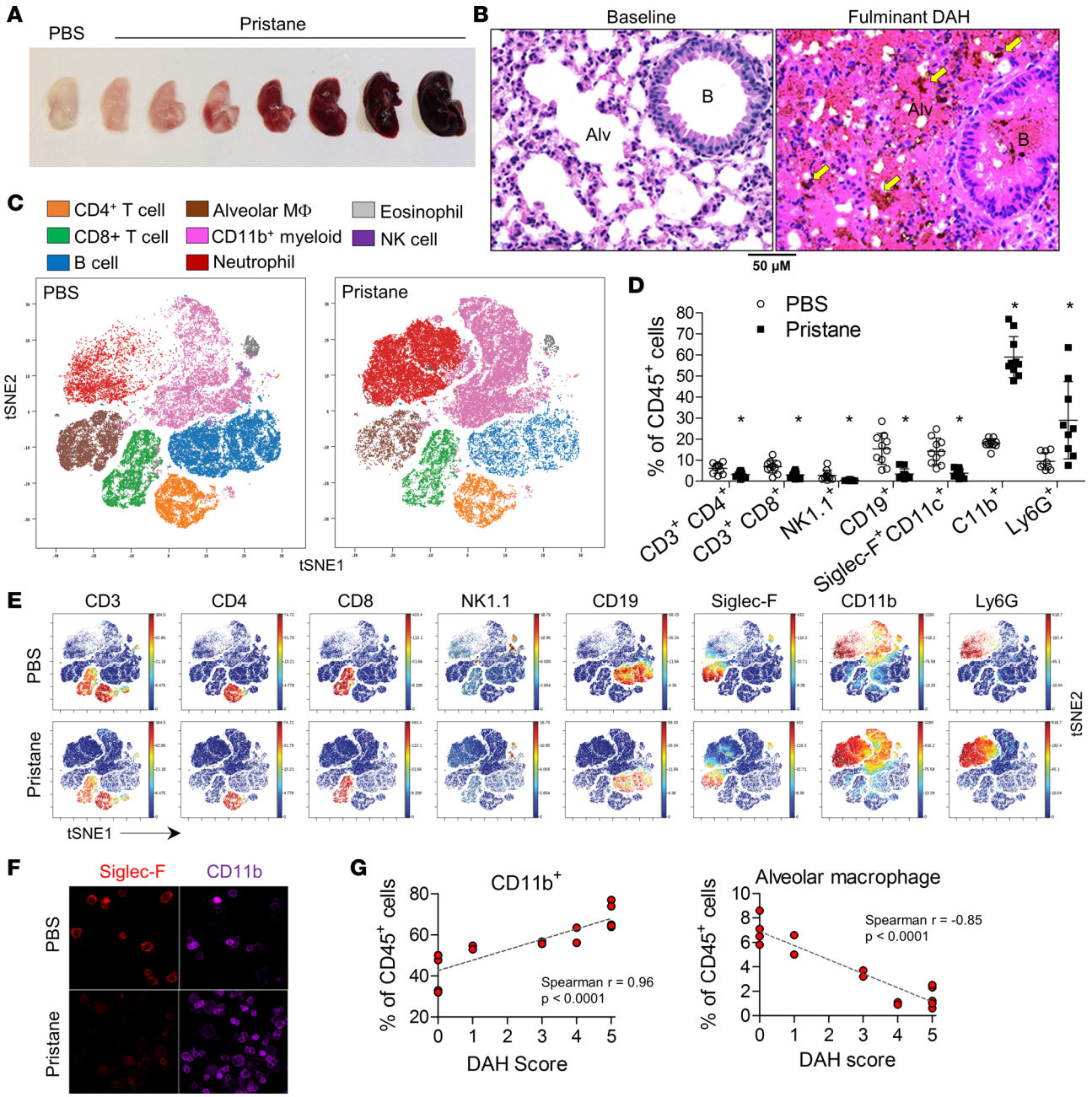

Figure 1. Mass cytometry analysis of lung immune cells in DAH. (**A**) Gross illustration of the spectrum of lung hemorrhage in C57BL/6 mice 2 weeks after pristane injection. (**B**) H&E staining of lung tissue from mice treated with pristane or PBS. B, bronchioles; Alv, alveolar space; arrows, hemosiderin deposits. (**C**) viSNE display of mass cytometry comparing isolated lung cells from PBS-treated and pristane-treated mice displayed by cell population identity (concatenated from 5 mice per group with equal sampling). (**D**) Quantification of lung cell populations as percentage of CD45$^+$ cells from mass cytometry analysis (n = 10 per group). (**E**) viSNE display of mass cytometry analysis by individual lineage identification markers. (**F**) Confocal microscopy of CD11b and Siglec-F expression in isolated lung cells (×100 magnfication). (**G**) Correlation of lung CD11b$^+$ myeloid cell expansion or Siglec-F$^+$CD11c$^+$ alveolar macrophage depletion with DAH severity score (n = 10). Data are representative of 3 independent experiments (**A**–**C**, **E**, and **F**) or pooled from 2 independent experiments (**D** and **G**). Statistical analysis was performed using unpaired Student's t test (**D**) and Spearman's correlation (**G**). *P < 0.05.

lung neutrophil and monocyte clusters and concomitant reduction of lymphocyte and alveolar macrophage populations (Figure 2D). To confirm the mass cytometry findings, we developed a gating strategy to accurately quantify lung neutrophils and monocytes in mice with DAH using flow cytometry (Supplemental Figure 2F). This method confirmed the increase of myeloid cells in the lungs of pristane-treated mice.

The role of neutrophils in pristane-induced DAH has been studied by several groups. Two groups found that antibody-mediated depletion of neutrophils either had no impact or exacerbated lung hemorrhage, while a more recent study noted mild improvement of DAH using the same approach (15, 20, 21).

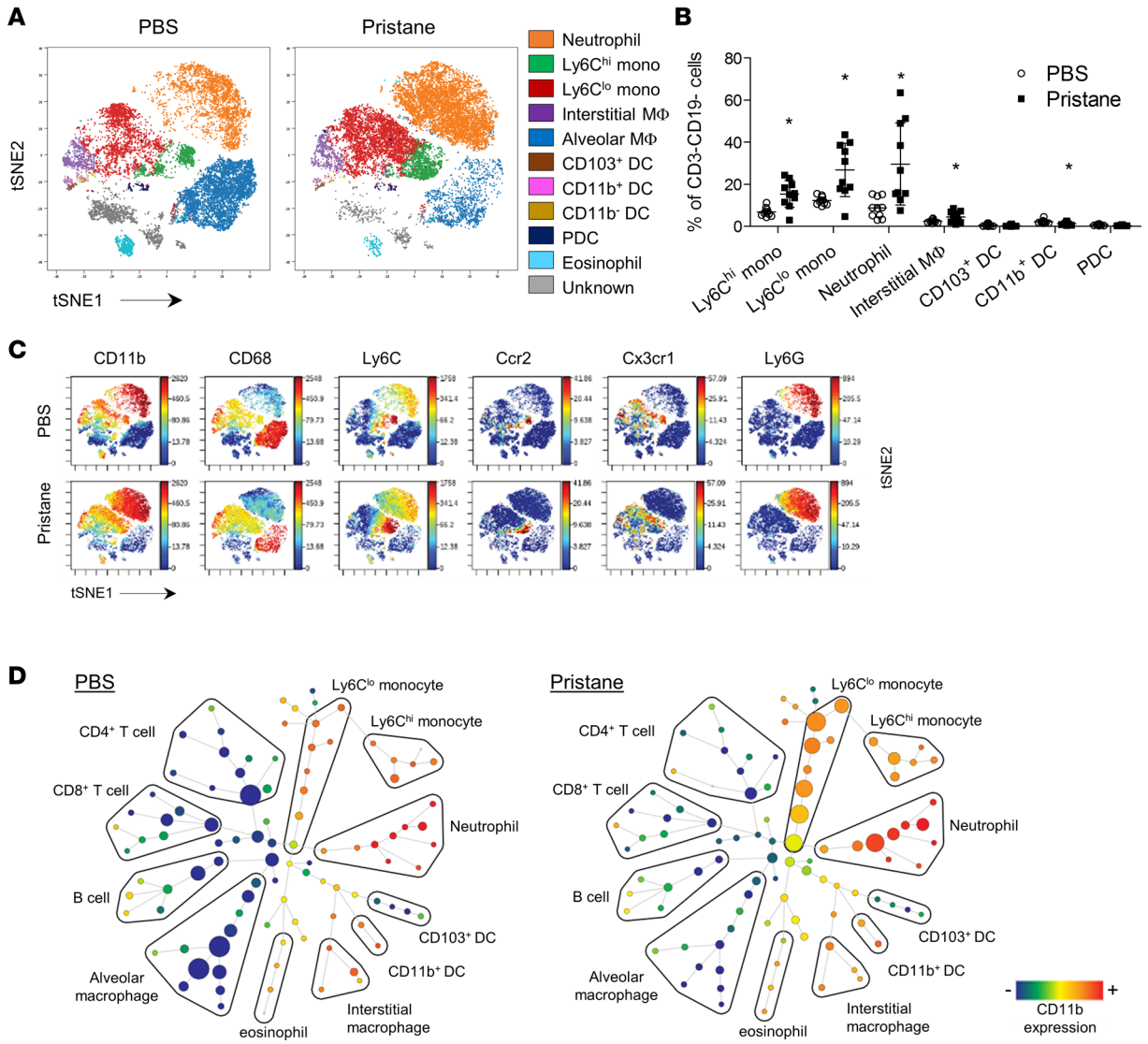

Figure 2. Expansion of monocytes and neutrophils in DAH. (**A**) Mass cytometry analysis of nonlymphoid cells ($CD45^+CD3^-CD19^-$ gate) in the digested lung tissue of PBS- or pristane-treated mice by viSNE analysis (concatenated from 5 mice per group with equal sampling). PDC, plasmacytoid DC. (**B**) Quantification of nonlymphoid populations ($n = 10$ per group) by mass cytometry. (**C**) viSNE display of mass cytometry analysis by individual lineage identification markers. (**D**) SPADE display of mass cytometry data with cluster size representing cell proportion and color reflecting CD11b expression levels. Data are representative of 3 independent experiments (**A**, **C**, and **D**) or pooled from 2 independent experiments (**B**). Statistical analysis was performed using unpaired Student's *t* test (**B**). $^*P < 0.05$.

We observed no marked difference in the severity of DAH in mice depleted of neutrophils using anti-Ly6G antibodies (Supplemental Figure 3, A and B). Therefore, we hypothesized that the infiltrating monocytes may play a key role in the development of DAH.

$Ly6C^{hi}$ monocytes are derived from myeloid progenitors in the bone marrow and egress to the periphery via the chemokine receptor Ccr2 (22). Under steady-state conditions, circulating $Ly6C^{hi}$ monocytes differentiate into the more mature $Ly6C^{lo}$ subset that expresses Cx3cr1 and patrols the vasculature (23, 24). In the setting of inflammation, $Ly6C^{hi}$ monocytes traffic to the inflamed tissue and differentiate into inflammatory or proresolving macrophages (25, 26). We confirmed the hematopoietic origin of lung monocytes in mice with DAH by bone marrow transplant studies (Supplemental Figure 3C). Interestingly, unlike the pattern seen in the bone marrow and peripheral blood, both monocyte subsets in the lung displayed high surface expression of Cx3cr1 (Supplemental Figure 3D). Consistent with the observation that neutrophil and monocyte recruitment induced by pristane is guided by distinct pathways (27, 28), neutrophil depletion by anti-Ly6G antibodies did not affect the influx of lung monocyte subsets (Supplemental Figure 3E).

Single-cell gene expression analysis in DAH. To understand the phenotype of myeloid cells in DAH, we performed droplet-based scRNA-Seq on immune cells ($CD45^+$) from digested lung tissue. More than 4000 cells from the lungs of pristane-treated mice with fulminant DAH and PBS-treated controls were successfully captured and sequenced. Unbiased K-means clustering of differentially expressed genes identified 8 major lymphoid and myeloid cell populations, which were marked by the differential expression of lineage-specific genes (Figure 3A and Supplemental Figure 4, A and B). Consistent with earlier data from mass cytometry, prominent expansion of monocytes and neutrophils as well as relative reduction in lymphocytes were observed with pristane treatment. scRNA-Seq analysis of mice with DAH also revealed the presence of immature neutrophils that expressed markers of bone marrow neutrophils and confirmed the depletion of alveolar macrophages (Figure 3A) associated with pristane treatment.

The monocyte cluster can be further stratified into $Ly6C^{hi}$ and $Ly6C^{lo}$ subsets (Supplemental Figure 4C). In addition to the expected differences in Ccr2 and Ly6C expression, lung $Ly6C^{hi}$ monocytes from pristane-treated mice showed upregulation of proinflammatory mediators, including serum amyloid and S100 proteins, compared with $Ly6C^{lo}$ counterparts (Figure 3B). In contrast, $Ly6C^{lo}$ monocytes exhibited prominent expression of proresolving mediators, such as IL-10, Marco, Irg1, and CD274/programmed cell death ligand 1 (PD-L1), suggesting that the 2 monocyte subsets may have different functions in pristane-mediated inflammation.

The gene expression profile of monocytes from pristane-treated mice was generally distinct from that of PBS-treated controls (Figure 3, C and D). Gene set enrichment analysis (GSEA) of lung monocyte subsets revealed enhancement of numerous immunologic pathways, including TNF-α, IL-6, and complement signaling, by pristane treatment (Figure 3E and Supplemental Table 2). These pathways have been implicated in the pathogenesis of pristane-induced inflammation (29, 30). In addition, neutrophils and residual alveolar macrophages from pristane-treated mice possessed a proinflammatory phenotype compared with their counterparts from PBS-treated controls (Supplemental Figure 4D). Significantly upregulated genes in lung neutrophils of pristane-treated mice included IL-1β and several IFN-inducible genes (*Iftim1*, *Ifi27l2a*, and *Isg15*; Supplemental Figure 4E). Taken together, data from scRNA-Seq corroborated the major findings from mass cytometry studies and revealed unique gene signatures corresponding to inflammatory pathways enriched in lung monocytes and macrophages in DAH.

Monocytes are essential for pristane-induced DAH. To examine the requirement for monocytes in DAH, we studied the impact of pristane on mice with monocyte deficiency. IFN regulatory factor 8 (Irf8) is a key transcription factor for monocyte differentiation from myeloid progenitors, and *IRF8* polymorphisms are risk alleles for human SLE (31–33). In line with previous studies (33, 34), monocytes were largely absent in the bone marrow of $Irf8^{-/-}$ mice, while neutrophil differentiation was enhanced (Supplemental Figure 5A). Importantly, $Irf8^{-/-}$ mice were protected from the development of DAH because only 2 of 30 mice exhibited lung hemorrhage, while the remainder displayed no gross or microscopic evidence of hemorrhage by 2 weeks after pristane treatment (Figure 4, A–C). In contrast, the majority of WT controls developed hemorrhage, and 7 of 25 succumbed to fulminant disease.

Mass cytometry of digested lung tissue revealed that the depletion of alveolar macrophages and relative reduction of lymphocyte populations associated with DAH were all attenuated in $Irf8^{-/-}$ mice (Supplemental Figure 5, B–D). Focused analysis of myeloid populations showed that lung monocyte populations in $Irf8^{-/-}$ mice, particularly $Ly6C^{hi}$ monocytes, were reduced at baseline and did not expand after pristane treatment (Figure 4, D and E). Conversely, the proportion of lung neutrophils was elevated in $Irf8^{-/-}$ mice at baseline and further increased with pristane treatment. As noted previously, plasmacytoid DCs (PDCs) and $CD103^+$ DCs were also reduced in $Irf8^{-/-}$ mice (Supplemental Figure 5D) (35–37). Therefore, in the setting of Irf8 deficiency where defective monocyte development results in compensatory granulocyte differentiation, mice are strongly protected against the development of pristane-induced DAH.

Irf8 regulates pristane-induced inflammation and autoimmunity. Because *IRF8* is also a susceptibility locus for human lupus (31–33), we asked whether Irf8 deficiency also affects the development of autoimmune manifestations induced by pristane. Past studies on pristane-induced autoimmunity have suggested a role of monocytes and DCs in producing IFN-Is, a group of antiviral cytokines important for the pathogenesis of human SLE (38, 39). As described previously (10), expansion of monocytes and neutrophils and upregulation of IFN-I–regulated genes, such as *Sca-1*, on lymphocytes were noted in the peripheral blood of WT mice 2 weeks after pristane treatment (Figure 5, A and B, and Supplemental Figure 6A). These features were abrogated in the peripheral blood of Irf8-deficient mice because monocyte subsets were nearly absent; neutrophils were expanded at baseline but unchanged with pristane treatment; and Sca-1 expression was not upregulated. In

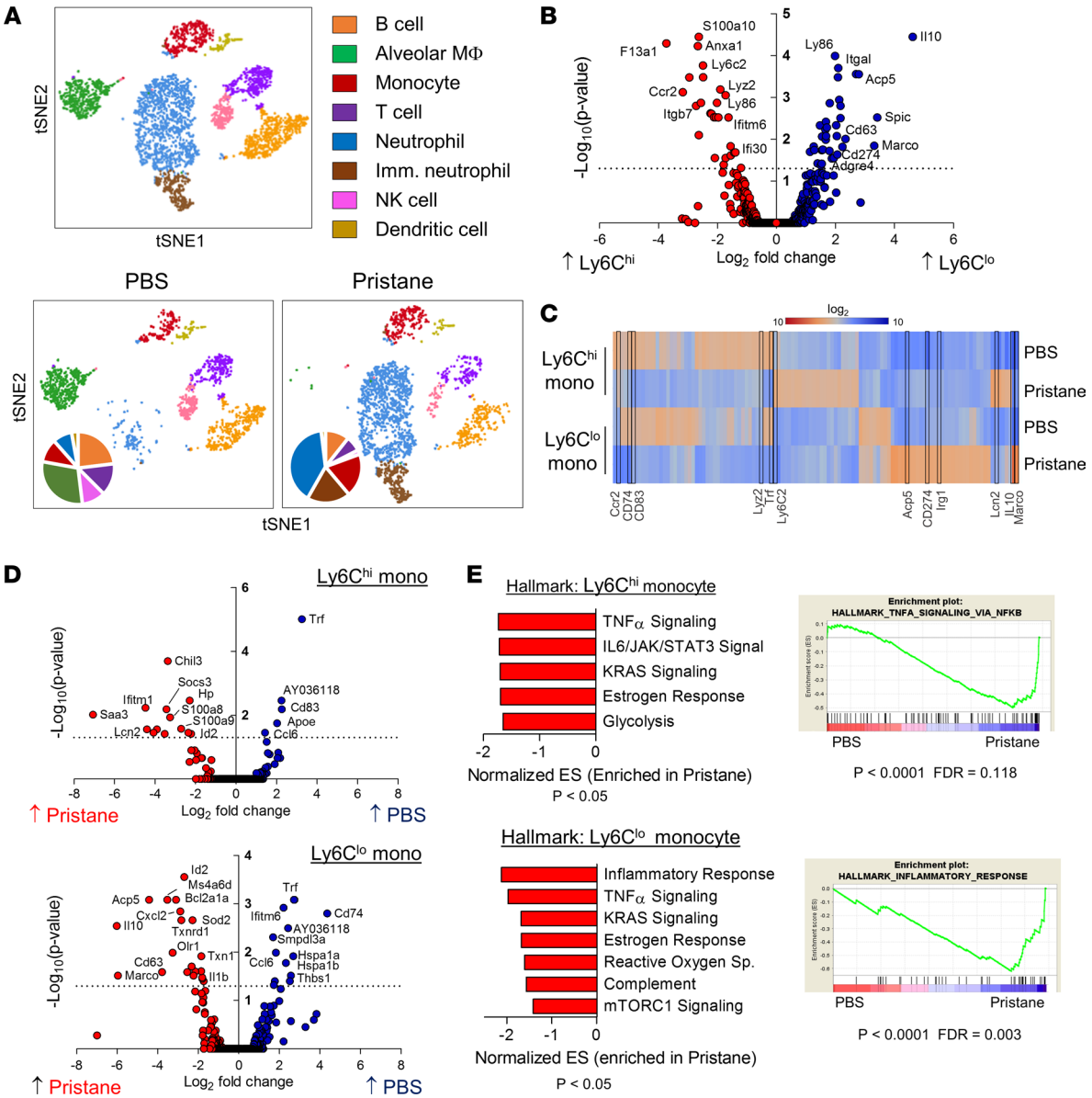

Figure 3. scRNA-Seq analysis of lung immune cells in DAH. (**A**) viSNE display of cell clustering based on gene expression by scRNA-Seq. Single cells (n = 4034 total) from the lungs of PBS- or pristane-treated mice (n = 2 per group) were pooled for analysis. (**B**) Illustration of differentially regulated genes in lung Ly6C^{hi} versus Ly6C^{lo} monocytes in mice treated with pristane. Dotted lines indicate threshold P value 0.05. (**C**) Heatmap display of differentially expressed genes in lung Ly6C^{hi} monocytes and Ly6C^{lo} monocytes in PBS- versus pristane-treated mice. (**D**) Illustration of differentially regulated genes in Ly6C^{hi} and Ly6C^{lo} monocytes of mice treated with PBS versus pristane. (**E**) GSEA of lung monocyte subsets in PBS- versus pristane-treated mice. Enriched gene sets (P < 0.05; FDR < 0.10) with pristane treatment were ranked by the normalized enrichment score (left), and representative enrichment plots are displayed (right). Statistical analysis was performed using established algorithms in Loupe Cell Browser (**B** and **D**) or GSEA software (**E**).

the peritoneum, where the inflammatory response to pristane is best characterized (38), infiltration of Ly6C^{hi} monocytes and depletion of residential peritoneal macrophages also diminished in the absence of Irf8 (Figure 5C). Similar to the lungs, the neutrophil response in the peritoneum was more prominent in Irf8$^{-/-}$ mice.

Importantly, the upregulation of IFN-inducible genes previously described in pristane-treated WT mice (10, 16) and in patients with lupus (40, 41) was abolished in the absence of Irf8, as revealed by bulk RNA-Seq of peritoneal exudate cells and confirmed by quantitative PCR (qPCR) (Figure 5D and Supplemental Figure 6, B and C). GSEA identified IFN-I signaling as the most downregulated pathway in Irf8$^{-/-}$ mice compared with WT controls (Figure 5E, Supplemental Table 3, and Supplemental Figure 6D). IFN-I signaling is required for the development of autoantibodies and kidney disease in this model (16). Indeed, the development of lupus-like features, including hypergammaglobulinemia, antinuclear antibodies (ANAs),

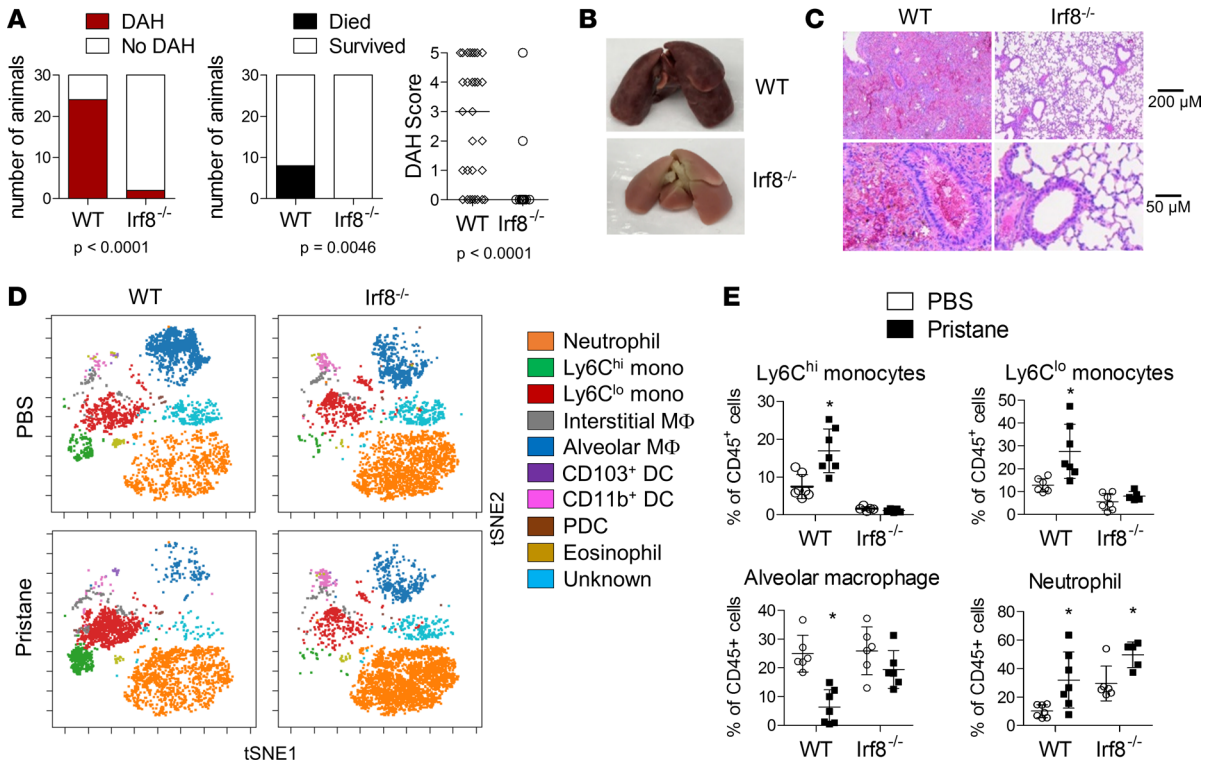

Figure 4. Irf8 is required for the development of pristane-induced DAH. (**A**) Incidence, mortality, and disease severity of DAH in WT versus Irf8$^{-/-}$ mice (n = 30 per group). (**B**) Representative gross illustration and (**C**) H&E staining of lung tissue of WT or Irf8$^{-/-}$ mice treated with pristane. (**D**) viSNE display and (**E**) quantitative comparison of lung myeloid populations (CD45$^+$CD3$^-$CD19$^-$ gate) from pristane-treated WT versus Irf8$^{-/-}$ mice (n = 6–8 per group) based on mass cytometry analysis. Data are representative of 3 independent experiments (**B**–**D**) or pooled from 3 to 4 independent experiments (**A** and **E**). Statistical analysis was performed using Fisher's exact test (**A**) and unpaired Student's t test (**D**). *P < 0.05.

anti-U1RNP antibodies, and glomerulonephritis as demonstrated by IgG and complement deposition, were all markedly reduced in Irf8$^{-/-}$ mice by 6 months after pristane treatment (Figure 5, F–I). These data illustrate an essential role of Irf8 for both DAH and the lupus-like disease pristane induces.

Disruption of monocytic chemokine signaling attenuates DAH development. Pulmonary capillaritis is a pathologic finding in human DAH as well as experimental DAH induced by pristane (3, 14). To understand whether the infiltration of monocytes is associated with vascular inflammation, we performed immunohistochemical staining of lung sections for Ccr2, which marks Ly6C^{hi} inflammatory monocytes. Whereas Ccr2$^+$ monocytes were scattered in the interstitium of PBS-treated controls, they congregated in the perivascular area and adhered to the vessel wall in mice with pristane-induced DAH (Figure 6, A and B). CCL2, a strong monocyte chemoattractant that interacts with CCR2, is markedly elevated in the bronchoalveolar lavage of patients with DAH (42). Correspondingly, lung tissue from mice with DAH, but not controls, also showed abundant expression of Ccl2 by immunohistochemistry (Supplemental Figure 7A). These data provide evidence for active monocyte migration and involvement in perivascular inflammation.

To address the role of monocyte migration in DAH, we studied 2 murine models with defective monocyte trafficking. Ccl2/Ccr2 signaling is required for egression of Ly6C^{hi} monocytes from the bone marrow and migration to the site of inflammation (43, 44). In Ccr2$^{-/-}$ mice treated with pristane, the incidence of DAH was greatly attenuated (in 5 of 20 mice vs. 14 of 20 for controls), and only 1 animal succumbed to disease (Figure 6C and Supplemental Figure 7B). As expected, lung Ly6C^{hi} monocytes were profoundly reduced while the Ly6C^{lo} subset also diminished by about 40% (Figure 6D).

On the other hand, Cx3cl1/Cx3cr1 signaling is classically linked to the homing of Ly6C^{lo} monocytes (23). However, both monocyte subsets in the lungs expressed high levels of Cx3cr1 (Supplemental Figure 3D), and the lower numbers of lung Ly6C^{hi} monocytes were previously noted in Cx3cr1$^{-/-}$ mice (45). After pristane treatment, the incidence of DAH was reduced by about 50% in Cx3cr1$^{-/-}$ mice (7 of 20 vs. 15 of 20 for controls), and 2 animals died from severe hemorrhage (Figure 6E and Supplemental Figure 7B). Compared with WT controls,

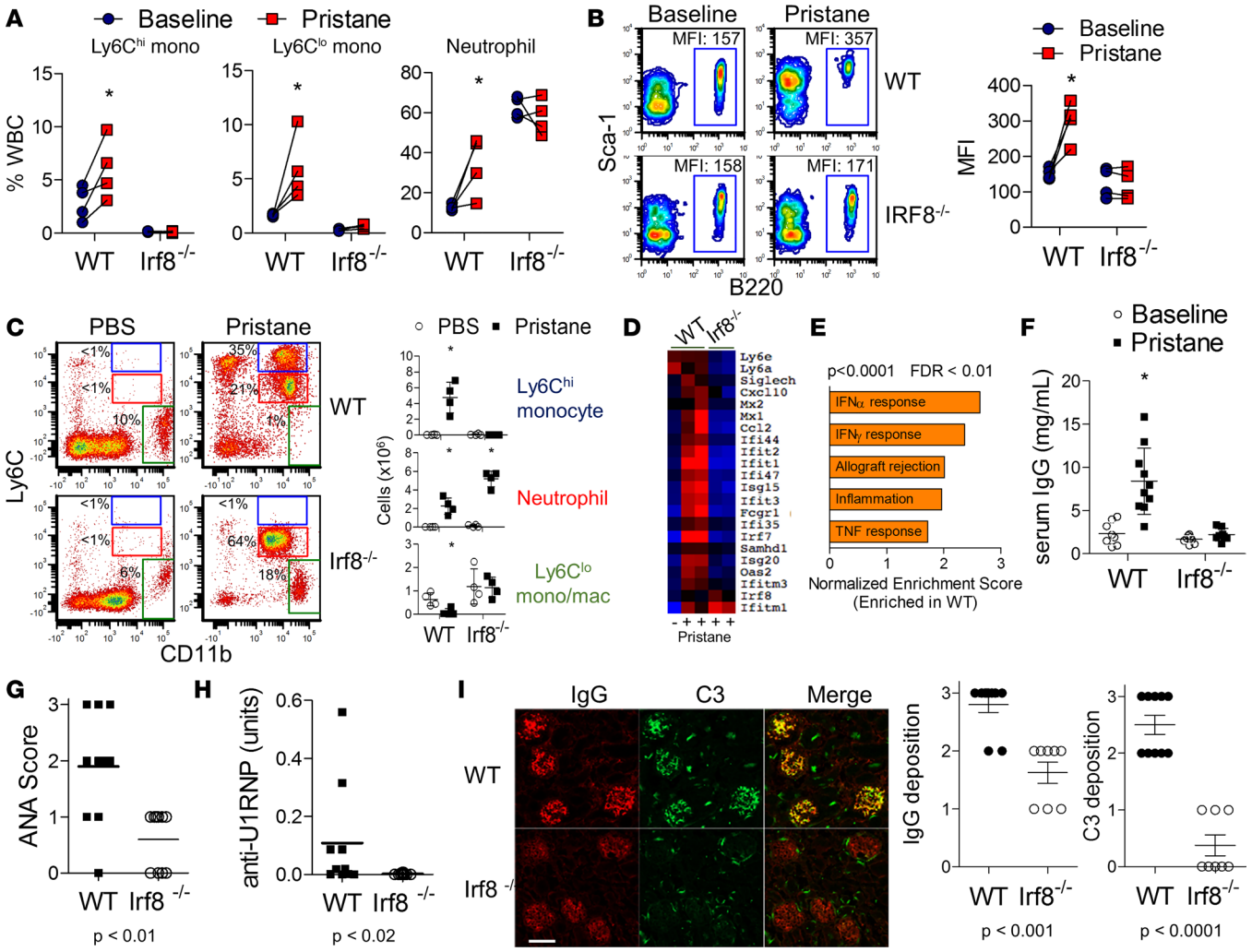

Figure 5. Irf8 is required for the development of pristane-induced autoimmunity. (**A**) Flow cytometry analysis of peripheral blood monocytes and neutrophils in WT and Irf8$^{-/-}$ mice in response to pristane treatment (n = 4 per group). (**B**) Flow cytometry analysis of Sca-1 expression on B lymphocytes (B220^{+}) in WT and Irf8$^{-/-}$ mice 2 weeks after pristane treatment (n = 4 per group). (**C**) Flow cytometry analysis and quantification of peritoneal exudate cells (n = 4 per group). Blue gate, Ly6C^{hi} monocytes; green gate, Ly6C^{lo} monocytes; red gate, Ly6C-intermediate Ly6G^{+} neutrophils. (**D**) Heatmap comparison of IFN-I–regulated gene expression. (**E**) GSEA of differentially regulated genes in WT and Irf8$^{-/-}$ mice 2 weeks after pristane treatment. Gene sets were filtered by nominal P < 0.0001 and FDR < 0.01 and ranked by normalized enrichment score. (**F**) Total serum IgG levels, (**G**) ANA levels by fluorescence microscopy, (**H**) anti-U1RNP levels by ELISA, and (**I**) immunofluorescence of glomerular IgG and C3 staining in WT and Irf8$^{-/-}$ mice (n = 8–10 per group) 6 months after pristane treatment. Scale bar: 100 μm. Data are representative of 2 independent experiments (**A**–**C**) or pooled from 2 independent experiments (**F**–**I**). Statistical analysis was performed using paired Student's t test (**A** and **B**) and unpaired Student's t test (**C** and **F**–**I**). *P < 0.05.

Cx3cr1-deficient mice showed more than 70% depletion of lung Ly6C^{lo} monocytes while Ly6C^{hi} monocytes were also reduced by 50% (Figure 6F). The remaining monocytes in Cx3cr1$^{-/-}$ and Ccr2$^{-/-}$ mice were deficient in the respective chemokine receptors (Supplemental Figure 7C), suggesting possible functional redundancy because deficiency of either molecule was not sufficient to eliminate monocyte homing to the lungs.

Because both chemokine receptors were important for the recruitment of Ly6C^{hi} and Ly6C^{lo} monocytes, these data could not determine the contribution of individual monocyte subsets in DAH. It was unclear whether Ly6C^{lo} monocytes migrate to the lungs independently or originate from migrated Ly6C^{hi} monocytes. We therefore isolated bone marrow Ly6C^{hi} monocytes from WT CD45.1 mice and injected the cells i.v. into pristane-treated Ccr2$^{-/-}$ recipients (Supplemental Figure 7D). Analysis of lung tissue after 24 hours showed that donor cells accounted for about 30% of Ly6C^{hi} monocytes (Supplemental Figure 7E). Moreover, about 20% of Ly6C^{lo} monocytes were also CD45.1^{+}, indicative of maturation from Ly6C^{hi} monocytes after cell transfer (46). Supporting this view, depletion of lung monocytes by clodronate liposomes led to repopulation of Ly6C^{hi} monocytes that subsequently downregulated Ly6C expression in the lungs (Supplemental Figure 7F).

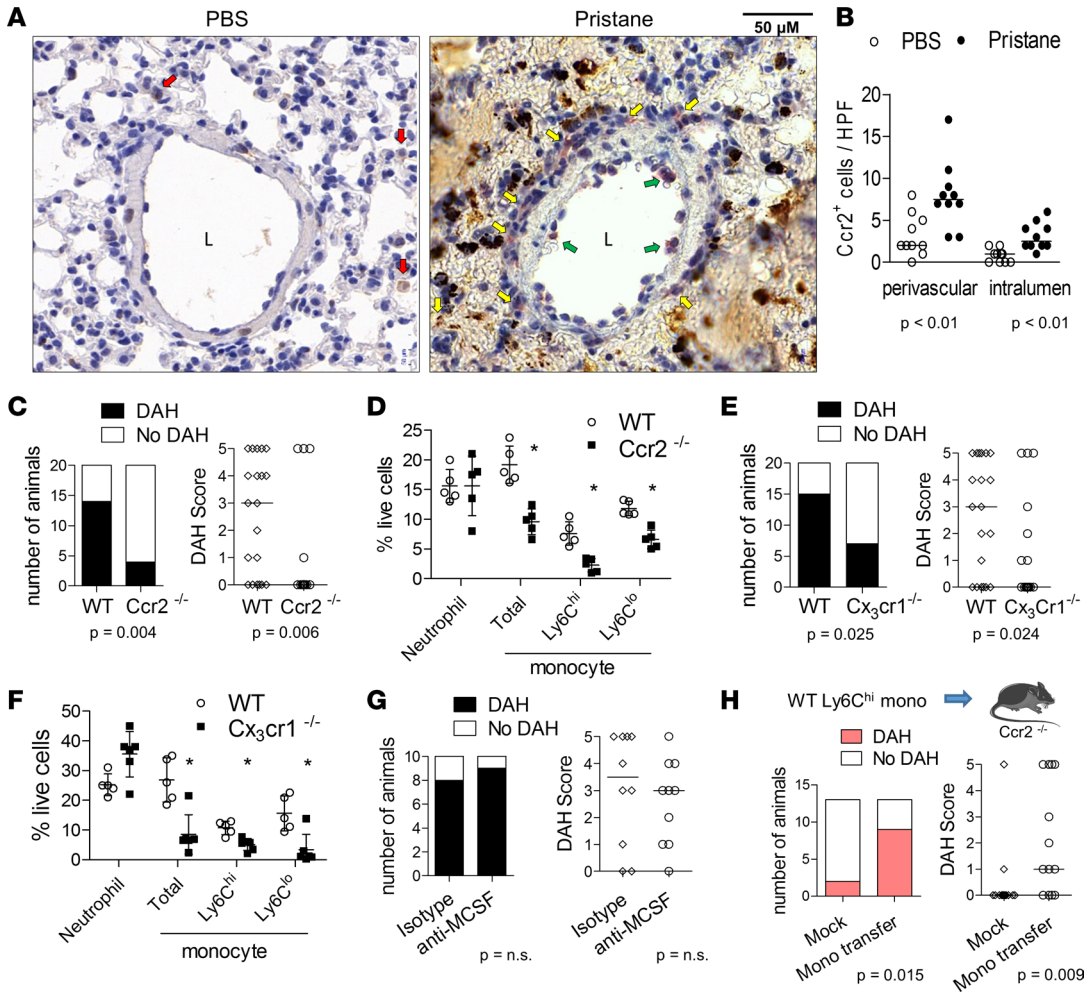

Figure 6. Attenuated DAH in mice deficient in monocyte chemoattractants. (**A**) Immunohistochemistry staining of Ccr2 in lung sections from mice treated with PBS or pristane. Red arrows: Ccr2$^+$ cells in the interface between capillaries and alveoli. Yellow and green arrows: Ccr2$^+$ cells in the perivascular region and inside the blood vessel lumen (L), respectively. Dark debris in the background represents hemosiderin deposits. (**B**) Quantitation of perivascular and intraluminal Ccr2$^+$ cells per ×40 high-power field (n = 10 fields/group). (**C**) DAH incidence and severity score of pristane-treated WT and Ccr2$^{-/-}$ mice (n = 20 per group). (**D**) Flow cytometry quantification of lung monocytes (n = 5 per group). (**E**) DAH incidence and severity score of pristane-treated WT and Cx3cr1$^{-/-}$ mice (n = 20 per group). (**F**) Flow cytometry quantification of lung monocytes (n = 5–7 per group) in WT and Cx3cr1$^{-/-}$ mice. (**G**) DAH incidence and severity score of pristane-treated WT mice given neutralizing antibodies against MCSF or isotype control (n = 10 per group). (**H**) DAH incidence and severity score of pristane-treated Ccr2$^{-/-}$ mice given purified bone marrow monocytes from WT mice or mock transfer with PBS (n = 13 per group). For all panels, analyses were performed 2 weeks after pristane treatment. Data are representative of 3 independent experiments (**A**, **B**, **D**, and **F**) or pooled from 2 to 3 independent experiments (**C**, **E**, **G**, and **H**). Statistical analysis was performed using Fisher's exact test (**C**, **E**, **G**, and **H**) and unpaired Student's t test (**B**, **D**, and **F**). *P < 0.05.

Isolation of sufficient numbers of Ly6C^{lo} monocytes to perform the parallel transplant experiment was challenging because the proportion of these cells is 10-fold lower compared with Ly6C^{hi} monocytes in the bone marrow. Using an alternative approach to address the contribution of migrating Ly6C^{lo} monocytes to DAH, we injected pristane-treated mice with neutralizing antibodies against macrophage colony–stimulating factor (MCSF; Csf1). MCSF signaling via Csf1r (CD115) is selectively required for the survival of Ly6C^{lo} monocytes (47). Depletion of peripheral blood Ly6C^{lo} monocytes, but not their Ly6C^{hi} counterparts or neutrophils, was confirmed in mice given anti-MCSF antibodies (Supplemental Figure 7G). Monocyte subsets in the lungs, however, were not affected by MCSF blockade. The incidence, severity, and mortality of pristane-induced DAH were similar between anti-MCSF and isotype antibody treatment (Figure 6G and Supplemental Figure 7H). These data favor Ly6C^{hi} monocytes as the primary monocyte subset that infiltrates the lungs and subsequently gives rise to Ly6C^{lo} monocytes.

Finally, we investigated whether replenishment of circulating Ly6C^{hi} monocytes in Ccr2$^{-/-}$ mice could restore the development of DAH. Contaminating neutrophils were absent in the purified monocyte prepa-

rations (Supplemental Figure 7D). Infusion of WT monocytes every 2 days drastically increased the incidence of DAH in Ccr2$^{-/-}$ mice (9 of 13 vs. 2 of 13 in mock transfer group; Figure 6H). These data further support a pathogenic role of inflammatory monocytes in DAH.

Discussion

DAH is a dangerous complication of autoimmune diseases with high mortality rate and few targeted treatment options (1, 3). Beyond its association with rheumatologic conditions, DAH can develop spontaneously or following hematopoietic stem cell transplant (48, 49). The contribution of immune cell subsets to the pathophysiology of the DAH condition is not well understood. Using pristane-induced inflammation as a model, we used mass cytometry to unambiguously identify a myeloid cell signature in DAH and explored the gene expression of infiltrating cells by scRNA-Seq. Based on these findings, we applied 3 transgenic strains and monocyte transfer studies to define a pathogenic role of monocytes in the development of DAH.

Two parallel subsets of monocytes are recognized in humans and mice (22, 23). Murine Ly6C^{hi} inflammatory monocytes correspond to human CD14^{+} "classical" monocytes while Ly6C^{lo} patrolling monocytes are similar to human CD16^{+} "nonclassical" monocytes. Both monocyte subsets are found in the lung tissue, and their location confers the unique capacity to survey danger signals in the vascular space as well as the alveolar space (45). Expanding on previous work that showed amelioration of DAH by systemic phagocyte depletion using i.p. injection of clodronate liposomes (15), our study specifically implicates monocytes as the pathogenic lineage. Defective monocyte development in Irf8$^{-/-}$ mice correlated with almost complete prevention of pristane-induced DAH. Both Ccr2- and Cx3cr1-deficient strains showed reduced recruitment of monocytes to the lungs, corresponding to partial protection against DAH.

It is notable that deficiency of either Ccr2 or Cx3cr1 affected both Ly6C^{hi} and Ly6C^{lo} monocytes. Data from our monocyte transfer studies suggest direct recruitment of circulating Ly6C^{hi} monocytes to the lungs, where they mature and attain the Ly6C^{lo} phenotype. In this context, decreased recruitment of Ly6C^{hi} monocytes in the absence of Ccr2 likely explains the concomitant reduction in Ly6C^{lo} monocytes. On the other hand, data from MCSF blockade argue against direct migration of circulating Ly6C^{lo} monocytes to the lungs via Cx3cr1 signaling in this model. Cx3cr1 is highly expressed by Ly6C^{hi} monocytes in the lungs and may play a role in their migration. The reduction of both lung monocyte subsets in Cx3cr1$^{-/-}$ mice has been noted previously (45), and interpretation may be confounded by the role of Cx3cl1/Cx3cr1 signaling on monocyte survival (50). Without a model of specific Ly6C^{lo} monocyte deficiency in the lungs, our studies could not conclusively establish the role of this monocyte subset in DAH.

A proinflammatory role of monocytes and macrophages in the pathogenesis of SLE is well recognized (51, 52). The monocyte transcription factor *IRF8* is a susceptibility gene in human SLE, but a mechanistic link has not been established (31, 32). In the NZB model of lupus, deficiency of Irf8 reduced autoantibody production and kidney pathology (35). These effects were thought to be related to defective PDC development, although the impact of monocyte deficiency was not examined. We show that Irf8 is critical to both DAH and manifestations of autoimmunity induced by pristane, including the development of IFN-I signature, autoantibodies, and glomerulonephritis. The effect on DAH is likely secondary to defective monocyte development because other models with disrupted IFN-I production or signaling remain susceptible to the lung disease (15). This view is corroborated by attenuated lung hemorrhage in Ccr2$^{-/-}$ and Cx3cr1$^{-/-}$ mice with defective monocyte migration. The contribution of Irf8 to the lupus-like disease is likely multifactorial because the transcription factor can perpetuate positive feedback of IFN-I signaling (53) in addition to regulating the development of monocytes and DCs, the primary sources of IFN-I in this model (38, 39). Whether human *IRF8* polymorphisms also affect the risk of DAH in SLE is an interesting topic for future investigation.

How monocytes participate in lung inflammation leading to vascular damage and subsequent hemorrhage requires further investigation. Histologic assessment localized Ccr2^{+} monocytes to the pulmonary vasculature, both in the perivascular space and adherent to the luminal wall. These findings suggest a potential role of monocytes in vascular inflammation, although direct mediators of vascular injury and hemorrhage remain to be identified. Although scRNA-Seq identified an enrichment of TNF signaling in monocytes, TNF$^{-/-}$ mice remain susceptible to the development of DAH (15). We find that key signaling pathways in innate immunity, including TLRs, IFN-I receptor, IL-1/IL-33 signaling, and activating Fcγ receptors, are also not required.

IgM and complement C3 are necessary for DAH, and the interplay of these immune mediators with lung monocytes will need further clarification. Whether monocytes express a receptor for IgM is controversial (54, 55). Interestingly, deficiency of either CD11b or CD18 is protective in pristane-in-

duced DAH (15, 20). Although these complement receptors are abundantly expressed by monocytes, interpretation of previous findings is confounded by their dual function as integrins crucial for the migration and function of many cell types.

Despite the similarities in histologic features with human DAH, whether pristane-induced DAH reflects the biology of SLE-associated DAH remains an open question. Lung pathology occurs within 2 weeks of pristane treatment, long before the development of IgG autoantibodies and glomerulonephritis. Moreover, alveolar capillaritis in human DAH is associated with neutrophilic infiltration of the alveolar septa and fibrinoid necrosis, suggesting a pathogenic role of neutrophils (3, 7). Although a prominent influx of neutrophils is also observed in pristane-induced DAH, the contribution of neutrophils to lung pathology is less clear. A previous study found no improvement of DAH following antibody-mediated depletion of neutrophils, while a separate study demonstrated severer DAH and greater mortality following neutrophil depletion (15, 20). In contrast, a recent study noted mild improvement of DAH severity and arterial oxygen saturation (56). We used the same approach to deplete neutrophils and found no marked difference in DAH severity, though we could not exclude a small effect. Neutrophil influx also does not correlate with DAH severity because lung neutrophil numbers were unaffected in Ccr2$^{-/-}$ and Cx3cr1$^{-/-}$ mice, while neutrophil abundance was increased in DAH-resistant Irf8$^{-/-}$ animals. Infusion of monocytes without contaminating neutrophils was sufficient to restore disease in Ccr2$^{-/-}$ mice. Further work is needed to determine the relative contribution of monocytes and neutrophils in the development of DAH.

Taken together, our work collectively suggests a pathologic role of inflammatory monocytes in DAH. Attenuated lung disease in mice with disrupted chemokine signaling raises the possibility of targeting monocyte chemoattractants as a novel therapeutic approach for DAH. Parallel to our finding of upregulated Ccl2 expression in pristane-induced DAH, analysis of bronchoalveolar lavage from patients with DAH after allogeneic transplant found the monocyte chemoattractant CCL2 to be the most significantly upregulated immune mediator (42). Antibodies that target the CCL2/CCR2 and CX3CL1/CX3CR1 axes in humans have been developed for inflammatory arthritis (57, 58). Because the outcome of DAH with available immunosuppressive therapies remains suboptimal, targeting of monocytes or monocyte chemoattractants may be a promising approach to treat this life-threatening pulmonary complication.

Methods

Animal studies. WT C57BL/6, Irf8$^{-/-}$ [B6(Cg)-Irf8tm1.2Hm/J], Ccr2$^{-/-}$ [B6.129(Cg)-Ccr2tm2.1Ifc/J], Cx3cr1$^{-/-}$ (B6.129P-Cx3cr1tm1Litt/J), and CD45.1 (B6.SJL-Ptprca Pepcb/BoyJ) mice were obtained from Jackson Laboratory. Tlr7$^{-/-}$, Tlr9$^{-/-}$, Myd88$^{-/-}$, Trif$^{-/-}$, TNF$^{-/-}$, FcR$\gamma^{-/-}$, IL-1$\alpha/\beta^{-/-}$, and ST2$^{-/-}$ mice were previously described (10, 59, 60). Male and female mice aged between 6 and 8 weeks received a single i.p. injection of 0.5 mL pristane (MilliporeSigma). Analysis of DAH was performed after 2 weeks as described by previous studies (13–15). Determination of autoantibodies, total IgG, and glomerular IgG and C3 deposits was performed after 6 months. For MCSF blockade and neutrophil depletion, 100 g of neutralizing antibodies against MCSF (clone 5A1), Ly6G (clone 1A8), or isotype control (BioXcell) were given i.p. every 2 days starting on the day of pristane treatment. For monocyte depletion by clodronate liposomes (Clo-Lip; Encapsula NanoSciences), 100 μL of Clo-Lip was given i.v. in mice 1 week after pristane treatment, and lung monocytes were analyzed after 48 or 72 hours.

Tissue processing and DAH scoring. For lung tissue digestion, freshly isolated lungs were minced and digested in RPMI with 10% fetal bovine serum and collagenase type IV (100 U/mL; MilliporeSigma) for 1 hour. Cells were collected by centrifugation, incubated with RBC lysis buffer, washed in PBS, and filtered twice using 40-μm filters. For histology, extracted lungs were fixed in 4% paraformaldehyde for 48 hours before paraffin embedding. Tissue embedding, sectioning, H&E staining, and immunohistochemistry were performed by ServiceBio Inc. using rabbit polyclonal antibodies against mouse Ccr2 or Ccl2. Scoring of DAH severity was based on visual approximation of the total area of hemorrhage (0 = no hemorrhage; 1 = 1%–20%; 2 = 21%–40%; 3 = 41%–60%; 4 = 61%–80%; 5 = >81%) from the isolated lungs. Each animal was scored by 2 independent investigators. In cases where the scores differed between the investigators, a third investigator served as the tiebreaker. Quantitation of glomerular C3 and IgG deposits and measurement of ANAs and anti–ribonuclear protein antibodies were performed as described (16).

Mass cytometry. Mass cytometry was performed by the Longwood Medical Area CyTOF core (Dana-Farber Cancer Institute, Boston, Massachusetts, USA) using a modified panel of metal-conjugated antibodies (18) as listed in Supplemental Table 1. Isolated cells were washed with Maxpar staining buffer (Fluidigm) and blocked

with anti–mouse CD16/32 (BioLegend) followed by incubation with the antibody cocktail for 1 hour. Cells were washed with staining buffer and incubated with cell intercalation solution for 1 hour followed by 2 additional washes with staining buffer. Mass cytometry data were normalized using EQ Four Element Calibration Beads (Fluidigm). SPADE and viSNE analyses were performed using Cytobank Premium (Cytobank Inc.).

Flow cytometry. The protocol for flow cytometry was previously described (61), and fluorophore-conjugated antibodies used are listed in Supplemental Table 1. In brief, cells were incubated with anti–mouse CD16/32, then stained with an optimized amount of primary antibody or the appropriate isotype control for 15 minutes at room temperature before washing and resuspending in PBS supplemented with 0.1% BSA. Samples were acquired using a Becton-Dickinson FACSCanto II flow cytometer and analyzed with FCS Express 5 software (De Novo Software).

Confocal microscopy. Isolated lung cells were fixed using 4% paraformaldehyde for 15 minutes followed by permeabilization using PBS with 0.2% saponin and 1% BSA for 30 minutes. After washing with PBS with 1% BSA and blocking in PBS with 5% rat serum, cells were incubated with fluorophore-conjugated primary antibodies (BioLegend) and Hoechst 33342 for 1 hour. Cells were washed in PBS with 1% BSA, cytospun onto slides, and mounted with coverslips using FluorMount (Thermo Fisher Scientific). Images were acquired using a Zeiss Axio Observer Z1 Inverted Microscope with Zeiss LSM 800 with Airyscan confocal system (Zeiss). Image processing was performed using ImageJ software (NIH).

Cell transfer. For bone marrow transplant, recipient CD45.1 mice were irradiated using 2 split doses of 5 Gy and given 2×10^6 bone marrow mononuclear cells (PBMCs) from CD45.2 mice. Engraftment was confirmed by FACS analysis of PBMCs after 4 weeks. For monocyte transfer, Ly6C^{hi} monocytes from the bone marrow of CD45.1 mice were purified by magnetic activated cell sorting using a monocyte isolation kit (Miltenyi Biotec) with greater than 85% purity. Then, 1.5×10^6 cells in 200 μL PBS or PBS alone (mock control) were given to recipient Ccr2$^{-/-}$ mice every 2 days by i.v. injection starting on the day of pristane injection.

qPCR. The protocol for qPCR was described previously (61). Total RNA was extracted from peritoneal exudate cells using RNeasy Mini Kit (Qiagen), and cDNA was synthesized using the Superscript III First-Strand Synthesis Kit (Thermo Fisher Scientific). qPCR was performed using RT2 SYBR Green Mastermix (Qiagen) with a StepOne thermocycler (Thermo Fisher Scientific). Amplification conditions were 95°C for 10 minutes, followed by 45 cycles of 95°C for 15 seconds and 60°C for 1 minute. After the final extension (72°C for 10 minutes), a melting-curve analysis was performed to ensure specificity of the products. Gene expression was normalized to β-actin, and expression relative to the sample with the lowest expression was calculated using the 2–ΔΔCt method. Primers used in this study were Irf7 (forward: CTTGCGCCAAGACAATTCAG; reverse: GAGGCTCACTTCTTCCCTATTT), Ifit1 (forward: TACAGCAACCATGGGAGAGA; reverse: ACTGGACCTGCTCTGAGATT), Isg15 (forward: AGAGTCGATCCAGTCTCTGA; reverse: CTTTAGGTCCCAGGCCATT), and Oas1L (forward: CCAACCAGAGAGTGGAAAGAA; reverse: CAAAGCAGCCTACCTTGAGTA).

RNA-Seq. RNA-Seq data were deposited in the National Center for Biotechnology Information's Gene Expression Omnibus (accession number GSE133083). The protocol for bulk RNA-Seq was described previously (61). In brief, RNA from peritoneal cells (1×10^5) was isolated using Qiagen RNeasy Micro Kit. RNA-Seq was performed using the Smart-Seq2 platform. Smart-Seq2 libraries were prepared by the Broad Technology Labs (BTL) and sequenced by the Broad Genomics Platform. Transcripts were quantified by the BTL computational pipeline (61). GSEA was performed using software v3.0 (Broad Institute) with the Molecular Signatures Database hallmark gene set collection (62). Hierarchical clustering analysis was performed using Cluster 3.0, and heatmaps were constructed using Java Treeview (63, 64). For scRNA-Seq, isolated leukocytes were enriched by flow cytometric sorting on CD45 positivity and resuspended in 0.4% BSA in PBS at a concentration of 1000 cells/μL. Then, 7000 cells were loaded onto a single lane (chromium chip, 10× Genomics) followed by encapsulation in lipid droplets (Single Cell 3′ kit V2, 10× Genomics) and library generation per manufacturer protocol. cDNA libraries were sequenced to an average of 50,000 reads per cell using Illumina Nextseq 500. scRNA-Seq reads were processed with Cell Ranger v2.1 (10× Genomics), which demultiplexed cells from different samples and quantified transcript counts per putative cell. Quantification was performed using the STAR aligner against the mm10 transcriptome. Data analysis was performed using Loupe Cell Browser (10× Genomics).

Statistics. For group comparisons, mean ± SD are displayed. For quantitative variables, differences between 2 groups were analyzed by unpaired Student's *t* test. Fisher's exact test was used for comparison of categorical variables. All tests were 2 sided, and $P < 0.05$ was considered significant. Statistical analyses were performed using Prism 5.0 software (GraphPad Software).

Study approval. These studies were approved by the Institutional Animal Care and Use Committee of Brigham and Women's Hospital (BWH; Boston, Massachusetts, USA).

Author contributions

PYL, NNM, and PAN conceived and designed the study. PYL, NNM, YH, AL, QW, PC, YL, JAL, SH, HZ, and WHR performed the experiments and acquired data. JAL and EYK provided reagents. PYL, NNM, KW, and PAN analyzed the data. PYL and PAN drafted the manuscript and all authors edited the manuscript. PYL and NNM contributed equally in the experimental work and data acquisition. The order of co–first authorship was determined by effort in drafting and revising the manuscript.

Acknowledgments

We thank the BWH Human Immunology Center for assistance with cell sorting, the BWH Single Cell Genomics Core for assistance with scRNA-Seq, and the Longwood Medical Area CyTOF core (supported by the Joint Biology Consortium) for assistance with mass cytometry. This work was supported by the NIH/National Institute of Arthritis and Musculoskeletal and Skin Diseases K08AR074562 (to PYL), R01AR44731 (to WHR), R01AR065538 (to PAN), and P30AR070253 (to PAN); a Lupus Research Alliance Target Identification in Lupus Grant (to PAN); a Rheumatology Research Foundation Investigator Award (to PYL); a Joint Biology Consortium Microgrant (to PYL); and a Lupus Foundation of American Gina M. Finzi Student Fellowship (to NNM). PAN was supported by the Fundación Bechara and the Arbuckle Family Fund for Arthritis Research.

Address correspondence to: Pui Y. Lee, Boston Children's Hospital, 300 Longwood Avenue, Boston, Massachusetts 02115, USA. Phone: 617.525.1084; Email: pui.lee@childrens.harvard.edu. Or to: Peter A. Nigrovic, Brigham and Women's Hospital, 60 Fenwood Road 6002-L, Boston, Massachusetts 02115, USA. Phone: 617.525.1031; Email: pnigrovic@bwh.harvard.edu.

1. Martínez-Martínez MU, Oostdam DAH, Abud-Mendoza C. Diffuse alveolar hemorrhage in autoimmune diseases. *Curr Rheumatol Rep*. 2017;19(5):27.
2. Zamora MR, Warner ML, Tuder R, Schwarz MI. Diffuse alveolar hemorrhage and systemic lupus erythematosus. Clinical presentation, histology, survival, and outcome. *Medicine (Baltimore)*. 1997;76(3):192–202.
3. Lara AR, Schwarz MI. Diffuse alveolar hemorrhage. *Chest*. 2010;137(5):1164–1171.
4. Andrade C, et al. Alveolar hemorrhage in systemic lupus erythematosus: a cohort review. *Lupus*. 2016;25(1):75–80.
5. de Prost N, et al. Diffuse alveolar haemorrhage: factors associated with in-hospital and long-term mortality. *Eur Respir J*. 2010;35(6):1303–1311.
6. Colby TV, Fukuoka J, Ewaskow SP, Helmers R, Leslie KO. Pathologic approach to pulmonary hemorrhage. *Ann Diagn Pathol*. 2001;5(5):309–319.
7. Mark EJ, Ramirez JF. Pulmonary capillaritis and hemorrhage in patients with systemic vasculitis. *Arch Pathol Lab Med*. 1985;109(5):413–418.
8. Travis WD, Colby TV, Lombard C, Carpenter HA. A clinicopathologic study of 34 cases of diffuse pulmonary hemorrhage with lung biopsy confirmation. *Am J Surg Pathol*. 1990;14(12):1112–1125.
9. Reeves WH, Lee PY, Weinstein JS, Satoh M, Lu L. Induction of autoimmunity by pristane and other naturally occurring hydrocarbons. *Trends Immunol*. 2009;30(9):455–464.
10. Lee PY, et al. TLR7-dependent and FcgammaR-independent production of type I interferon in experimental mouse lupus. *J Exp Med*. 2008;205(13):2995–3006.
11. Satoh M, Reeves WH. Induction of lupus-associated autoantibodies in BALB/c mice by intraperitoneal injection of pristane. *J Exp Med*. 1994;180(6):2341–2346.
12. Satoh M, Kumar A, Kanwar YS, Reeves WH. Anti-nuclear antibody production and immune-complex glomerulonephritis in BALB/c mice treated with pristane. *Proc Natl Acad Sci U S A*. 1995;92(24):10934–10938.
13. Barker TT, et al. Pathogenic role of B cells in the development of diffuse alveolar hemorrhage induced by pristane. *Lab Invest*. 2011;91(10):1540–1550.
14. Chowdhary VR, Grande JP, Luthra HS, David CS. Characterization of haemorrhagic pulmonary capillaritis: another manifestation of Pristane-induced lupus. *Rheumatology (Oxford)*. 2007;46(9):1405–1410.
15. Zhuang H, et al. Pathogenesis of diffuse alveolar hemorrhage in murine lupus. *Arthritis Rheumatol*. 2017;69(6):1280–1293.
16. Nacionales DC, et al. Deficiency of the type I interferon receptor protects mice from experimental lupus. *Arthritis Rheum*. 2007;56(11):3770–3783.
17. Spitzer MH, Nolan GP. Mass cytometry: single cells, many features. *Cell*. 2016;165(4):780–791.
18. Becher B, et al. High-dimensional analysis of the murine myeloid cell system. *Nat Immunol*. 2014;15(12):1181–1189.
19. Qiu P, et al. Extracting a cellular hierarchy from high-dimensional cytometry data with SPADE. *Nat Biotechnol*. 2011;29(10):886–891.
20. Shi Y, et al. Pristane-induced granulocyte recruitment promotes phenotypic conversion of macrophages and protects against

diffuse pulmonary hemorrhage in Mac-1 deficiency. *J Immunol*. 2014;193(10):5129–5139.
21. Jarrot PA, et al. Neutrophil extracellular traps are associated with the pathogenesis of diffuse alveolar hemorrhage in murine lupus. *J Autoimmun*. 2019;100:120–130.
22. Auffray C, Sieweke MH, Geissmann F. Blood monocytes: development, heterogeneity, and relationship with dendritic cells. *Annu Rev Immunol*. 2009;27:669–692.
23. Geissmann F, Jung S, Littman DR. Blood monocytes consist of two principal subsets with distinct migratory properties. *Immunity*. 2003;19(1):71–82.
24. Auffray C, et al. Monitoring of blood vessels and tissues by a population of monocytes with patrolling behavior. *Science*. 2007;317(5838):666–670.
25. Ginhoux F, Jung S. Monocytes and macrophages: developmental pathways and tissue homeostasis. *Nat Rev Immunol*. 2014;14(6):392–404.
26. Jakubzick CV, Randolph GJ, Henson PM. Monocyte differentiation and antigen-presenting functions. *Nat Rev Immunol*. 2017;17(6):349–362.
27. Lee PY, et al. IL-1α modulates neutrophil recruitment in chronic inflammation induced by hydrocarbon oil. *J Immunol*. 2011;186(3):1747–1754.
28. Lee PY, et al. Type I interferon modulates monocyte recruitment and maturation in chronic inflammation. *Am J Pathol*. 2009;175(5):2023–2033.
29. Richards HB, Satoh M, Shaw M, Libert C, Poli V, Reeves WH. Interleukin 6 dependence of anti-DNA antibody production: evidence for two pathways of autoantibody formation in pristane-induced lupus. *J Exp Med*. 1998;188(5):985–990.
30. Zhuang H, et al. Toll-like receptor 7-stimulated tumor necrosis factor alpha causes bone marrow damage in systemic lupus erythematosus. *Arthritis Rheumatol*. 2014;66(1):140–151.
31. Cunninghame Graham DS, et al. Association of NCF2, IKZF1, IRF8, IFIH1, and TYK2 with systemic lupus erythematosus. *PLoS Genet*. 2011;7(10):e1002341.
32. Lessard CJ, et al. Identification of IRF8, TMEM39A, and IKZF3-ZPBP2 as susceptibility loci for systemic lupus erythematosus in a large-scale multiracial replication study. *Am J Hum Genet*. 2012;90(4):648–660.
33. Tamura T, Nagamura-Inoue T, Shmeltzer Z, Kuwata T, Ozato K. ICSBP directs bipotential myeloid progenitor cells to differentiate into mature macrophages. *Immunity*. 2000;13(2):155–165.
34. Yáñez A, Ng MY, Hassanzadeh-Kiabi N, Goodridge HS. IRF8 acts in lineage-committed rather than oligopotent progenitors to control neutrophil vs monocyte production. *Blood*. 2015;125(9):1452–1459.
35. Baccala R, et al. Essential requirement for IRF8 and SLC15A4 implicates plasmacytoid dendritic cells in the pathogenesis of lupus. *Proc Natl Acad Sci U S A*. 2013;110(8):2940–2945.
36. Bajaña S, Turner S, Paul J, Ainsua-Enrich E, Kovats S. IRF4 and IRF8 act in $CD11c^+$ cells to regulate terminal differentiation of lung tissue dendritic cells. *J Immunol*. 2016;196(4):1666–1677.
37. Sichien D, et al. IRF8 transcription factor controls survival and function of terminally differentiated conventional and plasmacytoid dendritic cells, respectively. *Immunity*. 2016;45(3):626–640.
38. Lee PY, et al. A novel type I IFN-producing cell subset in murine lupus. *J Immunol*. 2008;180(7):5101–5108.
39. Nacionales DC, et al. Type I interferon production by tertiary lymphoid tissue developing in response to 2,6,10,14-tetramethyl-pentadecane (pristane). *Am J Pathol*. 2006;168(4):1227–1240.
40. Baechler EC, et al. Interferon-inducible gene expression signature in peripheral blood cells of patients with severe lupus. *Proc Natl Acad Sci U S A*. 2003;100(5):2610–2615.
41. Bennett L, et al. Interferon and granulopoiesis signatures in systemic lupus erythematosus blood. *J Exp Med*. 2003;197(6):711–723.
42. Vande Vusse LK, et al. Alveolar levels of immuno-inflammatory mediators in diffuse alveolar hemorrhage after allogeneic transplant. *Bone Marrow Transplant*. 2018;53(9):1206–1209.
43. Boring L, et al. Impaired monocyte migration and reduced type 1 (Th1) cytokine responses in C-C chemokine receptor 2 knockout mice. *J Clin Invest*. 1997;100(10):2552–2561.
44. Serbina NV, Pamer EG. Monocyte emigration from bone marrow during bacterial infection requires signals mediated by chemokine receptor CCR2. *Nat Immunol*. 2006;7(3):311–317.
45. Rodero MP, et al. Immune surveillance of the lung by migrating tissue monocytes. *Elife*. 2015;4:e07847.
46. Yona S, et al. Fate mapping reveals origins and dynamics of monocytes and tissue macrophages under homeostasis. *Immunity*. 2013;38(1):79–91.
47. MacDonald KP, et al. An antibody against the colony-stimulating factor 1 receptor depletes the resident subset of monocytes and tissue- and tumor-associated macrophages but does not inhibit inflammation. *Blood*. 2010;116(19):3955–3963.
48. Afessa B, Tefferi A, Litzow MR, Krowka MJ, Wylam ME, Peters SG. Diffuse alveolar hemorrhage in hematopoietic stem cell transplant recipients. *Am J Respir Crit Care Med*. 2002;166(5):641–645.
49. Yanik GA, et al. The impact of soluble tumor necrosis factor receptor etanercept on the treatment of idiopathic pneumonia syndrome after allogeneic hematopoietic stem cell transplantation. *Blood*. 2008;112(8):3073–3081.
50. Kim KW, et al. In vivo structure/function and expression analysis of the CX3C chemokine fractalkine. *Blood*. 2011;118(22):e156–e167.
51. Katsiari CG, Liossis SN, Sfikakis PP. The pathophysiologic role of monocytes and macrophages in systemic lupus erythematosus: a reappraisal. *Semin Arthritis Rheum*. 2010;39(6):491–503.
52. Li Y, Lee PY, Reeves WH. Monocyte and macrophage abnormalities in systemic lupus erythematosus. *Arch Immunol Ther Exp (Warsz)*. 2010;58(5):355–364.
53. Tailor P, et al. The feedback phase of type I interferon induction in dendritic cells requires interferon regulatory factor 8. *Immunity*. 2007;27(2):228–239.
54. Kubagawa H, et al. Identity of the elusive IgM Fc receptor (FcmuR) in humans. *J Exp Med*. 2009;206(12):2779–2793.
55. Lang KS, et al. Involvement of Toso in activation of monocytes, macrophages, and granulocytes. *Proc Natl Acad Sci U S A*. 2013;110(7):2593–2598.
56. Jarrot PA, et al. Neutrophil extracellular traps are associated with the pathogenesis of diffuse alveolar hemorrhage in murine

lupus. *J Autoimmun*. 2019;100:120–130.
57. Haringman JJ, et al. A randomized controlled trial with an anti-CCL2 (anti-monocyte chemotactic protein 1) monoclonal antibody in patients with rheumatoid arthritis. *Arthritis Rheum*. 2006;54(8):2387–2392.
58. Nanki T, Imai T, Kawai S. Fractalkine/CX3CL1 in rheumatoid arthritis. *Mod Rheumatol*. 2017;27(3):392–397.
59. Cunin P, et al. Megakaryocytes compensate for Kit insufficiency in murine arthritis. *J Clin Invest*. 2017;127(5):1714–1724.
60. Townsend MJ, Fallon PG, Matthews DJ, Jolin HE, McKenzie AN. T1/ST2-deficient mice demonstrate the importance of T1/ST2 in developing primary T helper cell type 2 responses. *J Exp Med*. 2000;191(6):1069–1076.
61. Lee PY, et al. The metabolic regulator mTORC1 controls terminal myeloid differentiation. *Sci Immunol*. 2017;2(11):eaam6641.
62. Liberzon A, Birger C, Thorvaldsdóttir H, Ghandi M, Mesirov JP, Tamayo P. The Molecular Signatures Database (MSigDB) hallmark gene set collection. *Cell Syst*. 2015;1(6):417–425.
63. de Hoon MJ, Imoto S, Nolan J, Miyano S. Open source clustering software. *Bioinformatics*. 2004;20(9):1453–1454.
64. Saldanha AJ. Java Treeview — extensible visualization of microarray data. *Bioinformatics*. 2004;20(17):3246–3248.